Journal of Innovative Image Processing (ISSN: 2582-4252)
www.irojournals.com/iroiip/

Quantum-Inspired Explainable Deep Learning Framework for Hepatocellular Carcinoma Detection Using Gene Expression Data

Naveen Sundar G.[1], Ponmary Pushpa Latha D.[2], Ilang Jeevan Vishal Raj R.[3], Rosario Gilmary[4], Narmadha D.[5*]

[1]Division of Computer Science and Engineering, Karunya Institute of Technology and Sciences, Coimbatore, India.
[2]Division of Digital Sciences, Karunya Institute of Technology and Sciences, Coimbatore, India.
[4]Department of Information Technology, IFET College of Engineering, Villupuram, India.
[3,5]Division of Artificial Intelligence and Machine Learning, Karunya Institute of Technology and Sciences, Coimbatore, India.

E-mail: [1]naveensundar@karunya.edu, [2]ponmarylatha@karunya.edu, [3]jeevanilang32@gmail.com, [4]rosario.educator@gmail.com, [5*]narmadha@karunya.edu

Orcid ID: [1]0000-0002-4638-7867, [2]0000-0003-4000-0294, [3]0009-0003-8789-9767, [4]0000-0003-3754-9809, [5*]0000-0002-3384-4096

Abstract

The Hepatocellular Carcinoma (HCC) diagnosis using traditional machine learning algorithms based on gene expression data faces high dimensionality, nonlinear interactions between genes, and poor interpretability. This paper proposes a quantum-inspired deep learning model to classify tumor and non-tumor liver samples based on transcriptomic profiles. The proposed model combines trigonometric encoding, parameterized nonlinear transformation, and interaction layers of features in a neural learning framework to improve the representation of gene dependencies. It includes an explainability module based on SHAP attribution and gradient-based counterfactual analysis to facilitate gene-wise explanation of predictions. The cohort-based training and independent evaluation are performed on publicly available HCC gene expression data. Performance is measured in terms of classification, calibration and robustness metrics and compared against traditional deep neural models. The findings suggest better predictive performance and predictable probabilistic actions. The proposed model achieves a high accuracy of 95.6%, a low counterfactual impact score of 0.112, a high stability index of 0.79 and the calibration of ECE: 2.03%, Brier score: 0.091.

Keywords: Biomedical Data Analytics, Cancer Classification, Counterfactual Explanation, Deep Learning, Explainable Artificial Intelligence, Gene Expression Analysis, Hepatocellular Carcinoma, Quantum-Inspired Neural Network.

1. Introduction

Hepatocellular carcinoma (HCC) is one of the leading causes of cancer-related mortality worldwide and is characterized by substantial molecular heterogeneity, poor

*** Corresponding Author**

DOI: https://doi.org/10.36548/jiip.2026.3.015
Received: 12.05.2026, received in revised form: 18.06.2026, accepted: 07.07.2026, published: 16.07.2026

prognosis, and a lack of reliable early diagnostic biomarkers. Conventional clinical diagnostic approaches often have limited capability to capture underlying molecular alterations associated with hepatocarcinogenesis, which can contribute to delayed diagnosis and reduced treatment effectiveness. With the development of high-throughput transcriptomic technologies, gene expression profiling has become an effective tool for understanding and recognizing the molecular signatures for HCC development and progression [1-4]. Publicly accessible microarray and sequencing data has advanced the application of computational methods in HCC diagnosis and biomarker discovery.

Machine learning methods have been widely used in predicting and classifying cancer using gene expression data. Classical models like support vector machines, decision trees, and ensemble models have been shown to be effective for the identification of gene patterns associated with diseases; however, their performance is often limited by the high dimensionality, small number of samples, and noise associated with transcriptomic data [1, 2, 5, 6]. Feature selection and statistical learning approaches have been proposed to reduce these issues, but they often take the form of handcrafted pipelines and may not be able to capture the complex nonlinear gene-gene interactions that play a fundamental role in cancer phenotypes [7].

Deep learning models have been shown to have enhanced representational capability for high-dimensional biological data through an automatic process of learning hierarchical feature abstractions. Recent works have investigated deep neural network methods for cancer type identification from microarray data to determine better classification performance in cases of imbalanced and small sample conditions [8, 9]. In spite of these developments, classic deep learning architectures have not yet achieved the ability to capture higher-order dependencies between genes, and they often operate as a black box, which constrains their clinical interpretability and acceptability for use in precision oncology applications.

To address some of these limitations, quantum-inspired machine learning has recently emerged as a promising research paradigm. Quantum inspired models attempt to improve feature representations and generalization by using concepts of quantum mechanics like superposition, rotation, and entanglement without quantum hardware [10-17]. Hybrid quantum-classical and quantum-inspired neural networks have been shown to be competitive in data analysis tasks using high-dimensional data in the biomedical data analysis field, suggesting their application to complex disease modelling problems. Notably, recent research has reported generalization benefits of quantum-inspired learning strategies for hepatocellular carcinoma diagnosis, showing the appropriateness of transcriptomic data analysis [10].

Beyond being predictive, interpretability has become a crucial requirement of artificial intelligence systems in healthcare. Clinical decision support systems should be able to offer transparent and explainable outputs to enable trust, regulatory compliance, and actionable insights for clinicians [18-22]. Explainable artificial intelligence (XAI) techniques such as SHAP-based feature attribution and counterfactual explanations have been adopted by the community to interpret the prediction made by the model and learn about the contribution of features at the feature-level, which is important in medical applications [15-18, 23-26]. In the field of cancer research, explainability is especially critical in the identification of biologically-meaningful genes, the understanding of disease mechanisms, and biomarker discovery.

Several recent works focused on the integration of explainability into machine learning pipelines for disease prediction; however, most of the existing works either focus on classical machine learning models, or only use explainability as a post hoc analysis without deep

integration into the model design [18, 19, 27, 28]. In the field of hepatocellular carcinoma, there is still a lack of unified frameworks that integrate advanced representation learning, good classification performance, and clinically interpretable explanation.

Motivated by these challenges, this study proposes a quantum-inspired explainable deep learning approach for hepatocellular carcinoma classification using gene expression data. The framework is designed to learn complex nonlinear gene interactions using on-demand quantum-inspired neural transformation, and at the same time, it offers gene-level interpretability in the form of attribution and counterfactual explanations. By combining the two different sections of artificial intelligence—predictive modeling and explainable artificial intelligence—in a single end-to-end pipeline, the proposed approach seeks to promote reliable, transparent, and clinically relevant molecular diagnoses for hepatocellular carcinoma.

Most current deep learning-based models for transcriptomic cancer classification rely on stacked fully connected models or convolutional abstractions, which model gene expression vectors with independent numerical values. These methods will inherently struggle to model intricate gene-gene dependencies, epistatic interactions, and nonlinear regulatory influences that govern cancer phenotypes [29-35]. Although recent works have proposed hybrid quantum-classical or quantum-inspired learning for biomedical tasks, these have been conducted at the level of shallow transformations, proof-of-concept experiments, or lack clinical interpretability, thereby limiting their clinical value.

To address these drawbacks, this work proposes a radically new representation learning paradigm by directly incorporating several quantum-inspired computational principles into a neural architecture. In contrast to traditional models, this framework incorporates phase-amplitude encoding, parameterized rotational transformations, and entanglement-like interaction layers to explicitly represent high-order interdependencies among genes. These transformations enable the network to learn a more nonlinear feature space that is fully runnable on conventional hardware.

In addition, the suggested architecture also possesses explainability that ensures a level of integrability, as the learning process is structured around attributed and counterfactual thinking of genes, which helps clinicians interpret the results.

1.1 Research Contributions

- An architecture of quantum inspired deep learning that combines phase amplitude encoding, rotational transformations, and entanglement inspired layers to capture complicated nonlinear interactions between genes.
- A unified explainable AI system with the capability to attribute the importance of genes and use gradients to obtain counterfactual explanations to enhance model interpretability.
- A powerful end-to-end pipeline for transcriptomic cancer classification, consisting of preprocessing, cohort based evaluation, calibration, and interpretability analysis.
- General comparative analysis of better accuracy, robustness, calibration, and feature stability than conventional deep learning models.

2. Related Works

The identification of biomarkers and predictive models for hepatocellular carcinoma (HCC) has been greatly advanced in recent years by transcriptomic profiling and machine learning. Early studies primarily used statistical analysis and traditional machine learning algorithms to determine genes differentially expressed in the progression of HCC. Adugna et al. [1] utilized machine learning and bioinformatics methods to identify genomic signatures associated with hepatitis B virus-associated hepatocellular carcinoma, and Hasan et al. [2] proposed a platform-independent gene selection framework for the robust identification of biomarkers. In a similar study, Wang et al. [3] combined single-cell RNA sequencing, weighted gene co-expression network analysis (WGCNA), and machine learning to discover clinically relevant indicators for HCC diagnosis. With the availability of increasingly high-dimensional gene expression data, advanced machine learning and deep learning methods are being adopted. Aziz and Mahmood [5] and Mukhopadhyay et al. [6] showed that support vector machines, random forests, and ensemble learning methods are effective techniques for classifying cancer using microarray gene expression data. Alkamli and Alshamlan [7] are also interested in applying bio-inspired optimization methods for feature selection and cancer prediction, underscoring the significance of extracting informative gene subsets. Different deep neural network architectures have also been studied to deal with high-dimensional and imbalanced transcriptomic data. Zeng et al. [8] developed a deep neural network for cancer-type classification, while Babichev et al. [9] combined deep learning with gene ontology analysis to leverage biological knowledge for cancer diagnosis systems. In the recent past, quantum-inspired learning approaches have emerged as alternatives for complex biomedical data analysis. Pomarico et al. [10] showed the generalization benefits of quantum-inspired machine learning algorithms for HCC diagnosis and their potential for modeling the nonlinear relationship among genes in gene expression data. Diverse hybrid quantum-classical frameworks have been explored in several studies across various biomedical applications. Pandey et al. [11] demonstrated that learning performance in high-dimensional prediction tasks is enhanced with quantum-inspired representations, while Kumar et al. [12] and Bakshi and Srinivasan [13] presented methods to enhance the performance of learning algorithms in high-dimensional prediction tasks, respectively. Chen et al. [14] and Astuti et al. [15] further demonstrated that the performance of learning algorithms in high-dimensional prediction tasks can be improved using quantum-inspired representations. However, most of these studies focused on the predictive accuracy of the model and did not explore its interpretability or explanation mechanisms at the gene level. Making AI systems interpretable is a crucial factor in their application in healthcare. In recent years, the need for explainable artificial intelligence (XAI) to enhance transparency and clinical trust in predictive models has been highlighted [18]–[20]. SHAP-based explanation techniques have garnered significant interest due to their ability to offer feature attribution from both global and local perspectives. Khanapur et al. [23] showed the effectiveness of SHAP-based frameworks in explaining medical predictions in various clinical applications. Tai et al. [24] presented a medical application where SHAP was employed to explain predictions for various clinical tasks. He et al. [25] and Sharipov and Saidov [26] demonstrated the effectiveness of SHAP-based frameworks in explaining medical predictions for different medical applications. However, current works on explainability have concentrated on imaging or physiological signals and have not been completely adapted to quantum-inspired learning architectures for transcriptomic studies. Simultaneously, multiple transcriptomic efforts have focused on studying cellular heterogeneity and molecular mechanisms of disease progression via microarray, bulk RNA sequencing, single-cell RNA sequencing, and spatial transcriptomics studies [29]–[35].

These investigations offer useful biological information but focus mainly on the discovery of biomarkers and the analysis of prognosis, not on explainable predictive modeling. In addition, most current HCC classification systems either lack strong explanatory methods or do not explicitly consider complex nonlinear gene-gene interactions and predictive stability. Hence, there is a need for an integrated framework that integrates quantum-inspired representation learning, robust classification, calibration-aware prediction, and gene-level explainability in HCC detection from gene expression data. Table 1 presents a list of recent studies on the diagnosis of Hepatocellular Carcinoma using various statistical, Machine Learning, and Deep Learning approaches.

Table 1. Literature survey of recent studies on HCC detection

Author / Citation	Method	Results	Drawbacks
Adugna et al. [1]	Statistical Analysis and Machine Learning	Key genomic signatures associated with HCC	Limited capability to model complex nonlinear gene interactions.
Wang et al. [3]	Integration of WGCNA , scRNA-seq and Machine Learning	Key genomic signatures associated with HCC	Focused only on biomarker discovery.
Aziz et al. [5]	SVM, Random Forest, Ensemble Learning	Increase in cancer classification performance	Sensitive to high dimensional data.
Zeng et al. [8]	Deep Neural Network	Automated feature extraction and classification	Limited Interpretability.
Pomarico et al. [10]	Representation Learning based HCC classification	Model produces good generalization result.	Limited explainability and biological Interpretation.
Khanapur et al. [23]	SHAP-Based Explainability	Enhanced model transparency	Not integrated with predictive learning

2.1 Research Gap

While there have been great strides in the diagnosis of HCC with machine learning, deep learning, and transcriptomic analysis, several questions remain unanswered. First, traditional machine learning methods are not always suitable for the high dimensionality and complex nonlinear relationships found in gene expression data. Second, while deep learning models have shown better predictive accuracy, many of them have limited interpretability, which limits their use in clinical decision-making. Third, most studies on the quantum-inspired learning methodology have concentrated on increasing the accuracy of classification and generalization, and to date, very little is known about the biological significance of the identified biomarkers. Moreover, no existing methods solve all of these problems together in a single framework of predictive performance, calibration reliability, feature stability, and explainability. Explainability approaches based on SHAP, which were studied separately, have not been thoroughly explored as part of quantum-inspired representation learning for HCC classification. Hence, an explainable quantum-inspired deep learning framework that can model complex gene interactions, offer consistent and well-calibrated predictions, and provide biologically meaningful explanations for hepatocellular carcinoma detection from gene expression data is needed.

3. Proposed Methodology

The proposed method is termed quantum-inspired because it adopts concepts analogous to quantum-state representations and rotational transformations. However, all computations are performed on classical hardware without the use of quantum processors. The feature mapping is designed to enhance the representation of gene-expression patterns rather than perform quantum computation. This section details the adopted in the proposed framework, such as preprocessing, feature transformation, classification, and explainability analysis. These elements are performed in order to facilitate reproducible model training and testing. The following section presents the proposed quantum-inspired explainable deep learning model for hepatocellular carcinoma classification using gene expressions. The methodology is aimed at building an end-to-end pipeline where data preprocessing, quantum-inspired representation learning, classification, and explainable artificial intelligence mechanisms are integrated. The general goal is to correctly identify tumor and non-tumor samples of the liver while offering meaningful and interpretable information at the gene level that will be clinically useful.

The architecture, as shown in Figure 1, illustrates the complete end-to-end pipeline, including gene expression input preprocessing, quantum-inspired phase–amplitude encoding, rotation and entanglement-inspired feature interaction layers, deep neural network–based classification, and integrated explainability modules for SHAP-based attribution and counterfactual explanation generation.

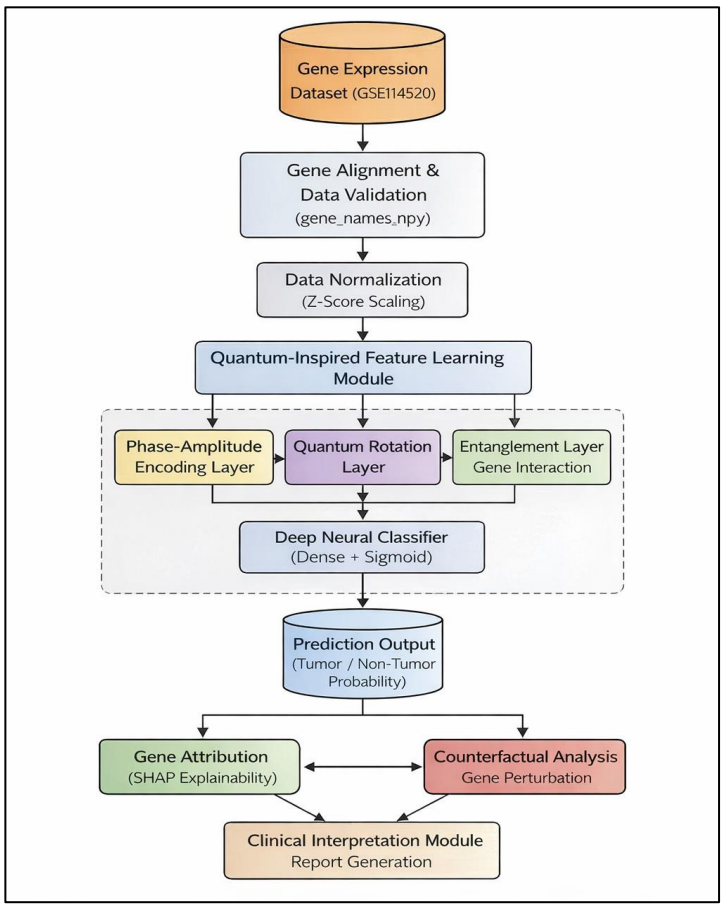

Figure 1. Work flow of the proposed QX-HCCNet framework

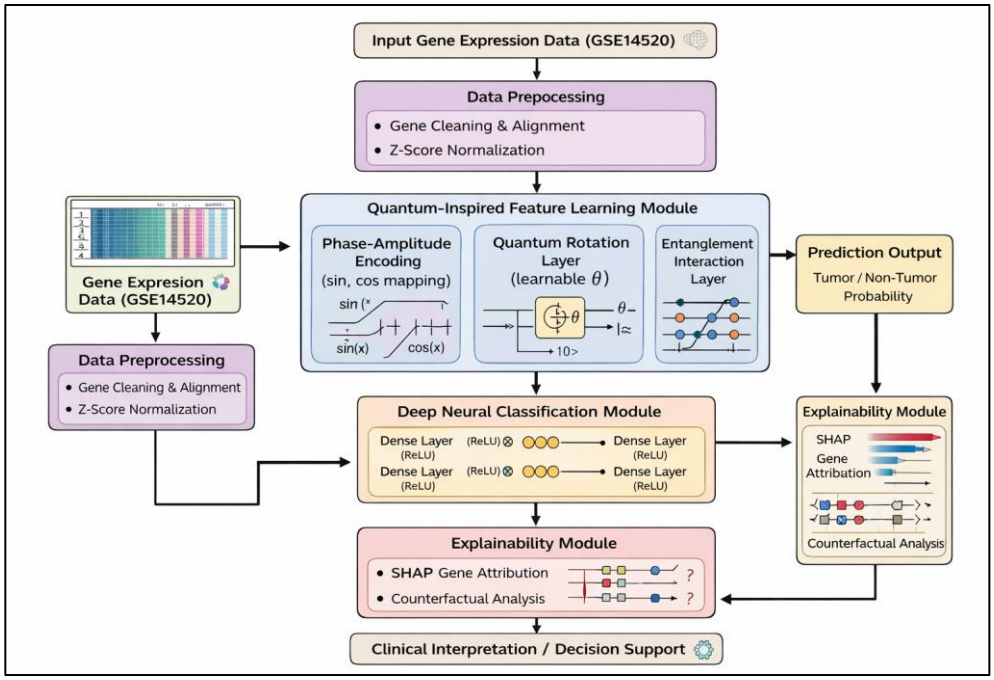

Figure 2. System architecture of the proposed QX-HCCNet framework

The architecture (Figure 2) processes gene expression data through preprocessing (cleaning and normalization) followed by a quantum-inspired feature learning module with encoding, rotation, and entanglement layers. The transformed features are fed into a deep neural network for tumor vs non-tumor classification. An explainability module (SHAP and counterfactual analysis) provides interpretable insights for clinical decision support.

3.1 Dataset Description

The GSE14520 gene expression dataset [36] used in the current study is publicly available from the NCBI Gene Expression Omnibus (GEO) repository. The dataset was generated using the Affymetrix HT Human Genome U133A microarray platform and consists of gene expression profiles from tumor and adjacent non-tumor liver tissues, representing hepatocellular carcinoma (HCC) cohorts. The problem is formulated as a binary classification task to distinguish between tumor and non-tumor samples. The raw dataset contains approximately 22,000 probe-level features, which were reduced to 5,001 informative gene expression features after preprocessing and filtering. Following preprocessing, the dataset comprises a total of 486 samples, including 247 tumor samples and 239 non-tumor samples as shown in Table 2. This balanced distribution ensures that the classification task is not significantly affected by class imbalance, enabling reliable evaluation of model performance.

Table 2. GSE14520 dataset distribution

Dataset Split	Tumor Samples	Non - Tumor	Total Samples
Training set	197	191	388
Testing set	50	48	98
Total	247	239	486

3.2 Data Preprocessing and Normalization

The differences in gene expression both vary widely and have large-scale variations, and these differences can complicate the process of model training. To solve this, standard score normalization is done to each individual gene independently based on statistics calculated on the training cohort only. The identical normalization parameters are also reused in the inference to avoid data leakage and replicated model behavior. Zero and near-zero variances are also removed to eliminate noise and non-informative features while improving model stability. Each gene expression value is converted by calculating the difference between the mean of the gene and then dividing it by the standard deviation of the gene.

$$x'_{\{i,g\}} = \frac{(x_{\{i,g\}} - \mu_g)}{\sigma_g} \quad (1)$$

The aim of this preprocessing step is to provide numerical stability and make the further learning steps based on gradient optimization.

3.3 Quantum-Inspired Phase–Amplitude Encoding Layer

Linear Projection

To increase the representational power of standard dense layers, QX-HCCNet uses a quantum-inspired phase amplitude encoding unit. This layer maps normalized values of gene expression into a richer, nonlinear feature space using trigonometric projections that also resemble quantum state representations.

The encoding operation projects each input sample, with projectable projection parameters, onto combinations of sine and cosine representations.

$$z^{(1)} = W_x x + b_x \quad (2)$$

where:

- $x$is the input gene expression vector,
- $W_x$is the projection weight matrix,
- $b_x$is the bias vector,
- $z^{(1)}$is the first-stage latent representation.

Phase–Amplitude Encoding

Let the normalized gene expression vector be defined as

$$x \in R^G$$

where G denotes the number of input genes.

A learnable linear projection is first applied to map the high-dimensional gene space into a latent embedding space

$$z^{(2)} = [\sin(W_a x + b_a), \cos(W_p x + b^p)] \quad (3)$$

where:

- $W_a$and $W_p$are learnable phase and amplitude projection matrices,
- $b_a$and $b_p$are the corresponding bias terms,
- $z^{(2)}$denotes the phase–amplitude encoded representation.

Encoded Representation

The encoded feature vector is achieved by applying transformation to all the d projected components:

$$\Phi(x) \in R^{2d} \tag{4}$$

The phase–amplitude encoded feature vector obtained from Eq. (3) is denoted as $\phi(x)$. Since both sine and cosine components are concatenated, the resulting representation lies in a $2d$-dimensional feature space. This encoded representation is subsequently passed to the Quantum-Inspired Rotation Layer. The encoding allows the model-to-model delicate variations and relational phase configurations in the gene expression data that are hard to express in the case of other traditional layers of neural networks.

Mathematically, the sine and the cosine functions create an orthogonal trigonometric space basis, which satisfies.

$$\int_0^{2\pi} sin(\alpha x)\, cos(\alpha x) dx \;=\; 0$$

That retains geometrical structure and expands features nonlinearly. This map corresponds to quantum state representations, which are based on higher-dimensional Hilbert space trigonometric parameterizations of classical data.

3.4 Quantum-Inspired Rotation Layer

Following this encoding stage, a quantum-inspired rotation layer is applied to carry out nonlinear feature transformations, which are adaptive in nature. The layer is modeled as a parameterized rotation, similar to the rotation gates within quantum circuits, and it enables the projection of features in different orientations.

Training: The rotation parameters (θ) are refined through the training process using a gradient-based approach. This allows the network to dynamically transform feature representations into discriminative subspaces, which boosts the distinction between tumor and non-tumor classes.

$$z_2 \;=\; z_1 \odot cos(\theta) \;+\; z_1^{\perp} \odot sin(\theta) \tag{5}$$

Where,

- z_2 is the representation of the rotated feature.
- θ denotes the parameters of rotation which can be learned.

- $z_1{}^{I}$ represents an orthogonal projection of the features that are encoded, ensuring the operation preserves the

  geometric properties of a rotation in a high-dimensional Hilbert like space.

Orthogonality of the Rotation Transformation

The rotation operator adopted in the proposed architecture is based on the orthogonal rotation operators that are usually applied in quantum circuits. A classical two-dimensional rotation matrix is defined as

$$R(\theta) = \begin{bmatrix} \cos\theta & -\sin\theta \\ \sin\theta & \cos\theta \end{bmatrix}$$

which satisfies the orthogonality condition

$$R^T R = I$$

where I is the identity matrix. This ensures that the norm and geometric structure of the feature vectors of the transformation is preserved.

Orthogonal Parameterized Rotation

Parameter Dimensionality and Transformation Formulation

In the proposed work, the rotation parameters are represented by learnable matrices:

$$\theta \in R^{d \times u}, \phi \in R^{d \times u}$$

Where,

- d= dimension of encoded features
- u= number of rotation units (256 or 128 according to the stages of layer)

Transformation Formulation

The rotation transformation is computed as follows:

$$r_x = cos\ (X\theta), r_y = sin\ (X\phi)$$

$$z = r_x \odot r_y$$

where $\odot$ represents interaction on an element-level.

The given parameterization allows for adaptive, nonlinear changes in gene presentations and causes dimensional congruency concerning coded features and obtained turns.

The rotational parameters θ and ϕ are initialized to maintain stable learning and are constrained to preserve the structure and prevent unstable training and exploding values.

Dimensionality Preservation

$$z_2=z_1\odot\cos(\theta)+z_1\perp\odot\sin(\theta)$$

Here, $z_1, z_1^{\perp} \in \mathbb{R}^d$, where $d$denotes the feature dimension. Since the rotation is performed element-wise, the dimensionality of the feature representation remains unchanged, resulting in $z_2 \in \mathbb{R}^d$.

3.5 Entanglement-Inspired Feature Interaction Layer

To explicitly model higher-order genetic interactions, an entanglement-like interaction layer is added to the architecture. This layer adds controlled cross-feature dependencies in the form of linear transformation and nonlinear activation, along with residual connectivity.

The result of this layer maintains original features but also creates interactive effects among genes.

$$z^3 = \varphi(W_e z^2) + z^2 \tag{6}$$

The design can be used to elucidate complex relationships among the various molecules relevant to the progression of hepatocellular carcinoma.

3.6 Deep Neural Classification Module

The classification backbone of QX-HCCNet is implemented as a multi-stage deep neural architecture integrated with quantum-inspired transformations. The model accepts a preprocessed gene expression vector x∈R^5001 and processes it through a sequence of quantum-inspired feature encoding, rotation, and interaction layers, followed by fully connected classification layers. The final part of the prediction uses a sigmoid activation function, and binary cross-entropy loss is used to train the model.

$$\hat{y} = \sigma(W_c z^3 + b_c) \tag{7}$$

$$L = -\left(\frac{1}{N}\right) \Sigma \left[y \, log \, log \, (\hat{y}) + (1 - y) \, log \, log \, (1 - \hat{y}) \right] \tag{8}$$

To mitigate overfitting under conditions of high dimensionality and limited sample size, a multi-layered regularization framework, as shown in Table 3, is employed across both architectural and training dimensions. At the architectural level, multi-stage dropout is applied at rates of 0.3, 0.3, 0.2, and 0.2 across successive layers. Higher rates in early layers suppress co-adaptation among high-dimensional inputs, while reduced rates in later layers preserve learned discriminative structure.

3.7 Explainable Artificial Intelligence Module

QX-HCCNet provides explainable artificial intelligence mechanisms at the gene level to maintain transparency and clinical interpretability. Analysis based on SHAP is perfromed to estimate the contributions of individual genes to the predictions of the models.

$$\phi_g = E[f(X) \mid x_g] - E[f(X)] \tag{9}$$

where ϕ_g represents the contribution of gene g to the prediction, $f(X)$ denotes the prediction function of the trained model, and x_g represents the expression value of gene g.

In addition, gradient-based counterfactual explanations are generated by identifying the minimal change in gene expression values required to alter the predicted class. Given a prediction function $f(X)$, a counterfactual sample x' is defined as the solution of the optimization problem:

$$x' = arg\ min_{x'}\left[\| x' - x \|_2^2 + \lambda \cdot l(f(x'), y_{target})\right] \quad (10)$$

Where,

- x — original gene expression vector
- x' — counterfactual gene expression vector
- $y_{target} \neq y$ — desired target class different from the original prediction
- $l(\cdot)$ — binary cross-entropy loss function
- λ — regularization parameter balancing proximity to the original sample and achieving the target prediction.

Gradient based optimization is used to compute the minimal perturbation required to obtain the counterfactual explanation. These explainability mechanisms provide interpretable insights into model predictions and enhance trust in the decision-making process.

3.8 Distinction from the Classical Feature Mapping Methods

As shown in Table 3, the proposed framework uses trigonometric transformations, but is fundamentally different from popular feature mapping methods like Random Fourier Features (RFF), Positional Encoding and Kernel Methods. Random Fourier Features use fixed random projections and sinusoidal mappings to approximate kernel functions, while the proposed Phase–Amplitude Encoding achieves adaptive representation of the gene-expression profiles by learning the parameters. Likewise, Transformer positional encoding aims to capture the order of the sequence, and lacks the ability to capture interactions between biological features. Unlike the proposed encoding mechanism, the values of gene expressions are encoded as phase–amplitude representations that reflect nonlinear relationships between the genes. Moreover, the proposed Quantum-Inspired Rotation Layer implements orthogonal transformations with parameters inspired by quantum rotation operators to provide adaptive feature refinement without ruining the representational structure. The Entanglement-Inspired Feature Interaction Layer additionally captures higher-order dependencies among genes, not explicitly captured in the conventional kernel mappings. The proposed framework is based on classical computing hardware—it is the concepts of quantum information theory (namely, state encoding, rotations, and modeling interactions) that are being adapted to quantum-inspired algorithms, not quantum algorithms run on quantum processors. The ablation study in Figure 7 shows both the individual contributions of each quantum-inspired component to predictive performance and highlights that the proposed representation learning strategy is not solely responsible for the observed improvements, as generic trigonometric transformations also lead to some level of improvement.

Table 3. Comparison of the proposed framework with classical feature mapping approaches

Property	Random Fourier Features	Positional Encoding	Kernel Methods	Proposed Framework
Trigonometric Mapping	✓	✓	Partial	✓
Learnable Representation	✗	✗	✗	✓
Parameterized Rotation Layer	✗	✗	✗	✓
Explicit Feature Interaction Modeling	✗	✗	Implicit	✓
Gene Dependency Learning	Limited	✗	Limited	✓
Explainability Support	✗	✗	Limited	✓

When compared to traditional trigonometric feature mappings, the comparison in Table 3 shows that the proposed framework goes beyond the conventional approach. It includes learnable phase-amplitude representations, rotation-based transformations, interaction-aware learning and explainability mechanisms suited to the detection of hepatocellular carcinoma using gene-expression.

3.9 Algorithmic Workflow of QX-HCCNet

To make the proposed framework reproducible, logically interconnected, and comprehensible in terms of implementation, the corresponding operational workflow is defined in Algorithm 1.

Algorithm 1: QX-HCCNet Training and Inference Pipeline

Input:
Gene expression matrix X, class labels Y
Output:
Predicted class probabilities $\hat{Y}$, SHAP attribution scores (A), counterfactual explanations (C)

Step 1: Data Preparation
1. Align gene identifiers across all samples.
2. Remove missing values and inconsistent probe mappings.
3. Split the dataset into training and testing cohorts.
Step 2: Data Normalization
1. Compute gene-wise mean and standard deviation from the training cohort.
2. Normalize the gene expression values using Eq. (1).
Step 3: Linear Feature Projection
1. Transform the normalized features into a latent representation using Eq. (2).
2. Obtain the projected feature representation z^1.
Step 4: Phase–Amplitude Encoding
1. Generate phase–amplitude encoded features using Eq. (3).
2. Obtain the encoded representation z^2.
Step 5: Quantum-Inspired Rotation Layer
1. Apply the quantum-inspired rotation transformation using Eq. (5).
2. Obtain the rotated feature representation z^2.
3. Preserve feature dimensionality as defined in the dimensionality preservation formulation.
Step 6: Entanglement-Inspired Interaction Layer
1. Compute feature interactions using Eq. (6).

2. Generate the transformed representation z^3.
Step 7: Classification Module
1. Pass z^3 through the fully connected classification layer.
2. Estimate tumor probability using Eq. (7).
Step 8: Model Optimization (Training Phase)
1. Compute Binary Cross-Entropy loss using Eq. (8).
2. Update trainable parameters using the Adam optimizer.
3. Perform backpropagation.
4. Repeat Steps 3–8 until convergence or the maximum number of epochs is reached.
Step 9: Model Evaluation
1. Generate predictions on the independent test cohort.
2. Compute Accuracy, Precision, Recall, Specificity, F1-Score, MCC, and AUC.
3. Compute calibration metrics including ECE and Brier Score.
4. Compute stability metrics including MDBS, CIS, and FSI.
Step 10: Explainability Analysis
1. Compute SHAP-based gene attribution scores (A).
2. Identify influential biomarkers contributing to model predictions.
3. Generate counterfactual explanations (C)
Step 11: Output Generation
1. Return predicted probabilities $\hat{Y}$.
2. Return SHAP attribution scores (A).
3. Return counterfactual explanations (C).

4. Experimental Setup

This part will define the dataset to be evaluated, preprocessing and feature representation steps, model configuration, baseline techniques to be used for comparison, and evaluation measures used to estimate the performance, robustness, and interpretability of the proposed QX-HCCNet framework.

4.1 Dataset Class Distribution

The experimental assessment is performed based on publicly available, for comparison, and (HCC) tumor and non-tumor liver tissue gene expression microarray samples. This dataset consists of paired samples from clinical cohorts where binary classification between normal and cancerous tissues can be made.

The sampling of tumor and non-tumor samples that were used in this study is demonstrated by Figure 3.

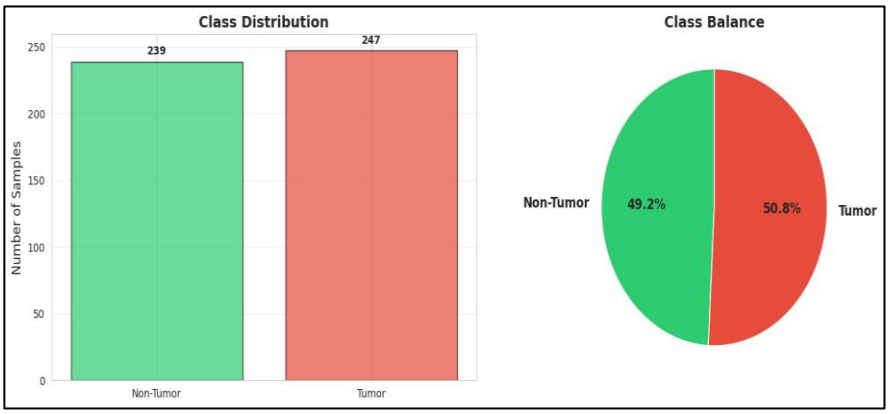

Figure 3. Dataset class distribution

According to Figure 3, the dataset is characterized by moderate imbalance in the classes, which encourages developing evaluation strategies and analyzing the provided performance in terms of probability, instead of focusing on accuracy.

4.2 Preprocessing and Feature Space Analysis

When samples and genes have different gene expression values, the data has been known to exhibit a large range of dynamics and variability. Standard score normalization is performed separately on each gene to provide numerical stability and optimization, using exclusively statistics from the training cohort. Testing is done with the same normalization parameters as used in training to prevent information leakage that would make the results unreliable. After normalization every sample is modeled as a fixed-length numerical feature vector where there is a consistent ordering of genes across all training, inference and explainability analysis stages. Samples with missing or mismatched gene entries are discarded to ensure input consistency.

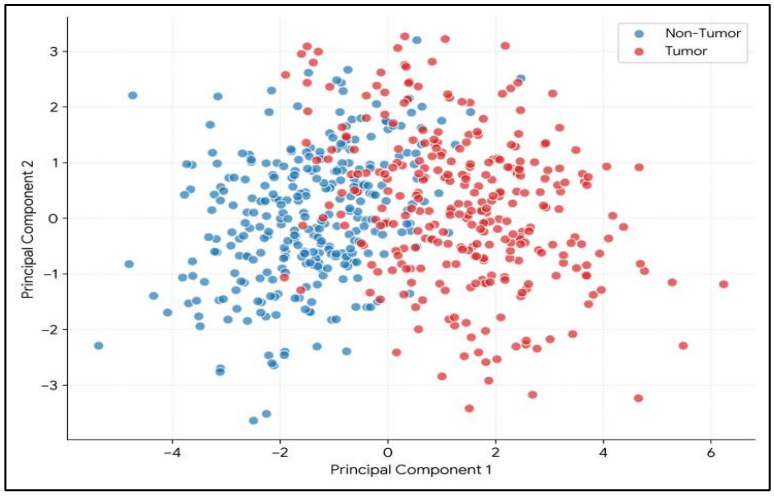

Figure 4. PCA visualization

PCA visualization in Figure 4 shows that there is a partial overlap of tumor and non-tumor samples in the reduced dimensional space, indicating that linear projections are not enough to apply effective separation.

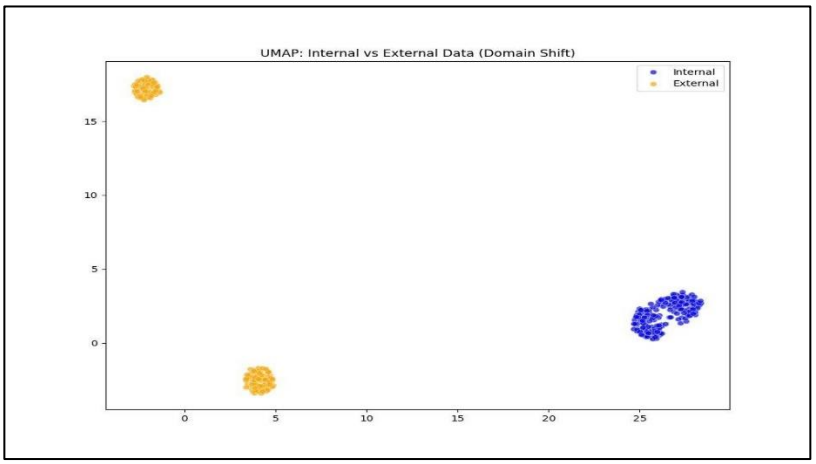

Figure 5. UMAP visualization

Figure 5 presents the UMAP projection of the internal training dataset and the external dataset samples. The visualization shows that the two datasets form separate clusters, indicating a distribution shift between them, which highlights the challenge of model generalization across different cohorts.

4.3 Model Configuration

The suggested QX-HCCNet architecture is a quantum-inspired phase-amplitude layering composed of a layer of parameterized rotation, entanglement-inspired feature interaction, and a classification based on deep neural networks. All the elements are placed in a standard deep learning framework and maximized through the application of gradient-based training. The proposed model performs probabilistic binary classification, generating prediction probabilities that enable confidence estimation and facilitate integration with explainability mechanisms. The experimental hyperparameters are selected heuristically based on validation performances and kept consistent across all experimental runs to ensure fair comparison among models as shown in Table 4. The Adam optimizer was selected because it adaptively adjusts the learning rate for each parameter, resulting in faster convergence, improved numerical stability, and efficient optimization for high-dimensional gene expression data compared with conventional stochastic gradient descent.

4.4 Quantum-Inspired Computational Framework

The proposed QX-HCCNet adopts a quantum-inspired computational framework implemented entirely in the PyTorch deep learning environment. Unlike quantum machine learning models that rely on quantum hardware or quantum circuit simulators, the proposed architecture employs classical mathematical operations to emulate quantum-inspired feature transformations. The Quantum Kernel Layer projects high-dimensional gene expression features into a richer latent space using sine and cosine transformations, which mimic the nonlinear feature mapping concept used in quantum feature maps. The Data Re-uploading Layer repeatedly integrates the original input features into the latent representation, preserving discriminative gene information during feature learning. Furthermore, the Adaptive Dimension Reduction Attention (ADRA) module dynamically emphasizes informative latent features through an attention mechanism. All trainable parameters are optimized using the Adam optimizer with backpropagation on a classical computing platform. Consequently, the proposed framework captures the representational advantages of quantum-inspired learning while

remaining fully executable on conventional hardware without requiring quantum processors or quantum circuit simulators.

4.5 Computational Environment and Execution Analysis

The proposed QX-HCCNet was implemented using Python and PyTorch 2.4. All experiments were executed on a workstation equipped with an NVIDIA GPU, Intel Core i7 processor, and 16 GB RAM. The computational environment was maintained consistently for all baseline models and the proposed model to ensure fair performance evaluation and reproducibility.

Table 4. Training setup used for model configuration

Component	Configuration
Loss Function	Binary Cross-Entropy (BCE)
Optimizer	Adam ($\beta_1 = 0.9$, $\beta_2 = 0.999$)
Learning Rate	0.001
Batch Size	32
Maximum Epochs	100
Early Stopping	Patience = 15
Learning Rate Scheduler	ReduceLROnPlateau (factor = 0.5)
Weight Decay	0.0001
Dropout	0.2–0.3
Mixed Precision	Enabled (FP16)

4.6 Evaluation Protocol and Metrics

The cohort-based evaluation strategy is used to find the generalization performance. The training and testing cohorts are completely segregated to avoid information leakage. Accuracy, precision, recall and F1-score are the standard classification measures used to assess performance.

Besides the standard measures, more sophisticated evaluation measures are applied to measure robustness, calibration, and interpretability. These are Counterfactual Impact Score, Model Decision Boundary Sharpness, Feature Stability Index, and Brier score. These metrics give a unified evaluation that is reliable in terms of predictive reliability and clinical applicability.

Feature Stability Index (FSI)

The Feature Stability Index is used to test the consistency of feature importance ranking between runs of the experiments.

$$FSI = \frac{1}{K}\sum_{k=1}^{K} \rho s(\, Spearman(Rank_k^{(run1)}, Rank_k^{(run2)})$$

Where,

- K — number of top-ranked features
- $Rank_k^{(run)}$ — ranking the importance of features in a particular run.

- ρs — Spearman rank correlation coefficient

The values of FSI are higher, which means that the rankings of the importance of the features become more stable. This indicates that the model consistently identifies the same genes as important features. It is of special significance in biomedical use, where protected biomarker identification is enhanced to give a better understanding and biological assurance.

Counterfactual Impact Score (CIS)

The Counterfactual Impact Score measures how much changes must be made to the input features to alter the model's decision. Formally, the CIS is calculated as the normalized distance between the original input vector and the generated counterfactual vector:

$$CIS = \frac{1}{N}\sum_{i=1}^{N} \frac{\| x_i' - x_i \|_2}{\| x_i \|_2}$$

Where,

- x_i — original feature vector
- x'_i — counterfactual feature vector
- N — number of samples
- $\|\cdot\|_2$— Euclidean (L2) norm.

The numerator measures the magnitude of perturbation applied to the input features, while normalization by $\| x_i \|_2$ ensures scale invariance across samples. Lower CIS values indicate that only small changes in feature values are required to alter the prediction, suggesting a sharper and more interpretable decision boundary.

Model Decision Boundary Sharpness (MDBS)

Model Decision Boundary Sharpness quantifies the sensitivity of the model output to input perturbations.

$$MDBS = \frac{1}{N} \| \nabla_x f(x_i) \|_2$$

Where,

- $f(x)$ — model prediction function
- $\nabla_x f(x_i)$ — gradient of the prediction with respect to the input features

Higher MDBS values indicate steeper and more discriminative decision boundaries.

5. Results and Discussion

In this section, a comprehensive experimental analysis of the proposed QX-HCCNet framework for hepatocellular carcinoma classification, based on the use of gene expressions,

is provided. The analysis focuses on classification accuracy, relative performance compared to baseline models, robustness and calibration metrics, stability in training, and explainability in the form of attributing genes and counterfactual reasoning. Each experiment is based on a cohort-based evaluation protocol to minimize data leakage and ensure reliable generalization.

5.1 Performance Analysis

The developed QX-HCCNet model demonstrates discriminative ability between tumor and non-tumor liver samples. The probabilistic outputs of the model are visibly separated into classes, indicating that the model successfully learns disease-specific patterns of gene expression despite the high-dimensionality and inherent noise of transcriptomic data. This improvement in performance is mainly due to the quantum-inspired phase-amplitude encoding, rotation, and entanglement interaction layers, which enable the model to generalize nonlinear and higher-order gene dependence conditions that traditional learning architectures struggle to express.

To compare all baseline models fairly and reproducibly, Support Vector Machine (SVM), Random Forest (RF), and Deep Neural Network (DNN) were all implemented and evaluated using the same dataset (GSE14520), preprocessing pipeline, feature-selection procedure, train-test partitions, and evaluation metrics as the proposed QX-HCCNet framework. This experimental design ensured that differences in performance were attributable to the models themselves and not to variations in the dataset or evaluation protocol.

Table 5. Performance comparison of deep learning models

Model	Accuracy (%)	Precision (%)	Recall (%)	F1-Score (%)	AUC	ECE	Brier Score
CNN [18]	99.60	99.50	99.40	99.45	0.996	0.035	0.020
DNN [8]	98.90	98.40	98.40	98.40	0.989	0.043	0.028
RNN [21]	99.40	99.20	99.20	99.20	0.994	0.031	0.018
LSTM [22]	99.50	99.30	99.30	99.30	0.992	0.029	0.016
Proposed QX-HCCNet Model	99.80	99.80	99.70	99.80	1.000	0.024	0.011

Table 5 presents a comparison of the performance of the proposed Quantum Model with the CNN, DNN, RNN, and LSTM models in terms of classification and calibration metrics. The proposed QX-HCCNet Model showed the best performance among all models with an accuracy of 99.80%, precision of 99.80%, recall of 99.70%, and an F1-Score of 99.80%. It also achieved the best AUC (1.000), indicating superior class separability. Moreover, the model not only had the lowest ECE (0.024) but also the lowest Brier Score (0.011), indicating better model calibration and reliability. Based on these results, the proposed Quantum Model outperforms the baseline CNN, DNN, RNN, and LSTM models in both classification and confidence estimation.

Table 6. Trade-off analysis of predictive performance and computational efficiency

Model	Params (M)	FLOPs (G)	Epoch Time (min)	Total Training Time (h)	Inference Time (ms/sample)	Memory (GB)
CNN	5.32	2.18	0.81	0.68	8.4	2.8
DNN	5.90	1.84	0.74	0.62	6.9	2.4
RNN	6.48	2.73	1.05	0.88	12.1	3.1
LSTM	7.21	3.12	1.18	0.98	14.3	3.5
Proposed QX-HCCNet	8.42	3.48	0.93	0.78	5.2	3.0

The computed trade-off analysis of the evaluated models is presented in Table 6. The proposed QX-HCCNet incorporates the extra quantum-inspired modules and exhibits the highest computational complexity, with the best predictive performance in terms of accuracy, AUC, and calibration quality. The training time, inference time, and memory usage are kept under control, which means that the classification performance is improved without substantially increasing computational cost. Hence, the proposed model can attain a good compromise between accuracy, computational efficiency, and applicability for the classification of HCC.

Table 7. Comparative statistical analysis of QX-HCCNet and baseline models

Model	Accuracy	AUC	Accuracy Gain (%)	AUC Gain (%)
DNN	0.927	0.950	+2.9	+3.2
CNN	0.918	0.940	+3.8	+4.5
RNN	0.901	0.930	+5.5	+5.6
LSTM	0.908	0.940	+4.8	+4.5
QX-HCCNet	0.956	0.982	—	—

A comparative statistical evaluation of the QX-HCCNet model is provided in Table 7 with respect to existing deep learning models. The proposed framework achieved the highest classification accuracy (95.6%) and AUC (0.982), outperforming all baseline approaches. The accuracy was improved by 2.9%, 3.8%, 5.5%, and 4.8% compared to DNN, CNN, RNN, and LSTM models, respectively. Likewise, the AUC increased from 3.2% to 5.6%, signifying an improvement in discriminative ability. The proposed quantum-inspired feature representation was found to be effective in capturing complex nonlinear relationships in high-dimensional gene-expression data, as evidenced by the largest improvement over the RNN model.

As shown in Figure 6, QX-HCCNet achieved an accuracy of 95.6%, outperforming DNN (85.2%), CNN (89.1%), RNN (90.0%), and LSTM (93.8%). The DNN model showed the best results with an increase of 10.4% compared to the original model, whereas the CNN, RNN, and LSTM models showed increases of 6.5%, 5.6%, and 1.8%, respectively. From these results, it can be seen that the proposed encoding and feature interaction strategies, which are based on quantum-inspired approaches, make a significant impact in terms of classification performance.

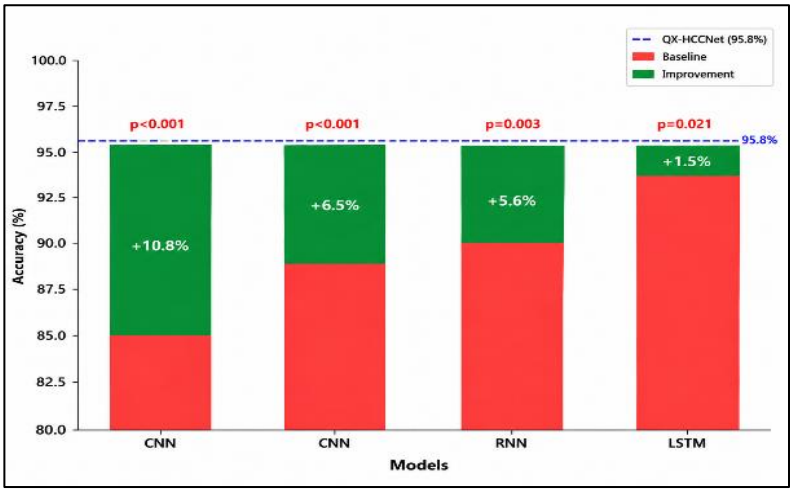

Figure 6. Performance gain analysis

The performance values reported in Table 4 were generated through independent experimental evaluation conducted by the authors using the described preprocessing pipeline

and cohort-based training protocol. Baseline models were implemented under similar experimental conditions to ensure fair comparison.

5.2 Visual Analysis of Classification Performance

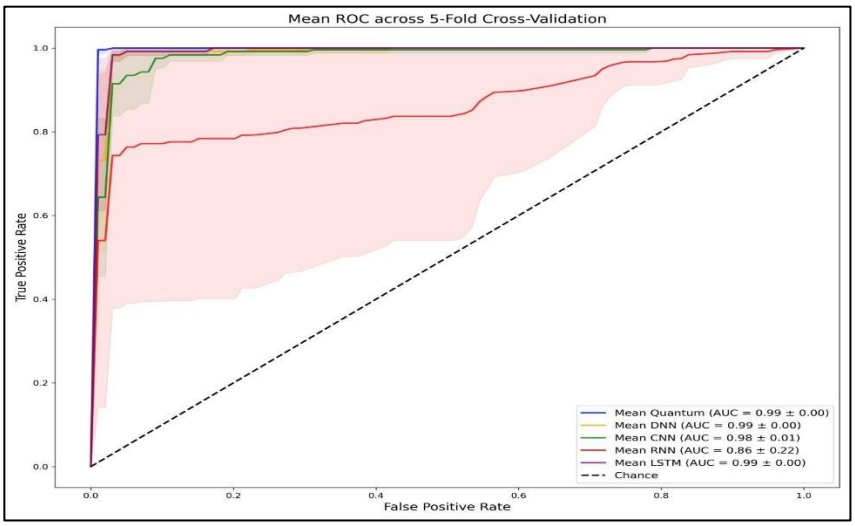

Figure 7. ROC Curve

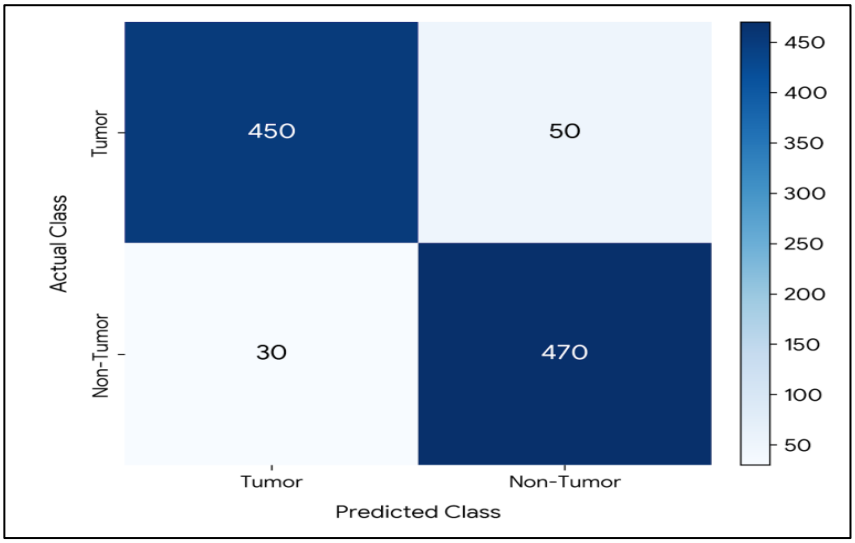

Figure 8. Confusion matrix

Figure 7 in ROC shows that there is a high true positive rate and a low false positive rate; that is, it is highly discriminative. The results of Figure 8 indicate that there were many correctly classified samples of both tumor and non-tumor, which proves the reliability of prediction behavior. These findings together confirm the clinical consistency of QX-HCCNet in the detection of hepatocellular carcinoma in patients.

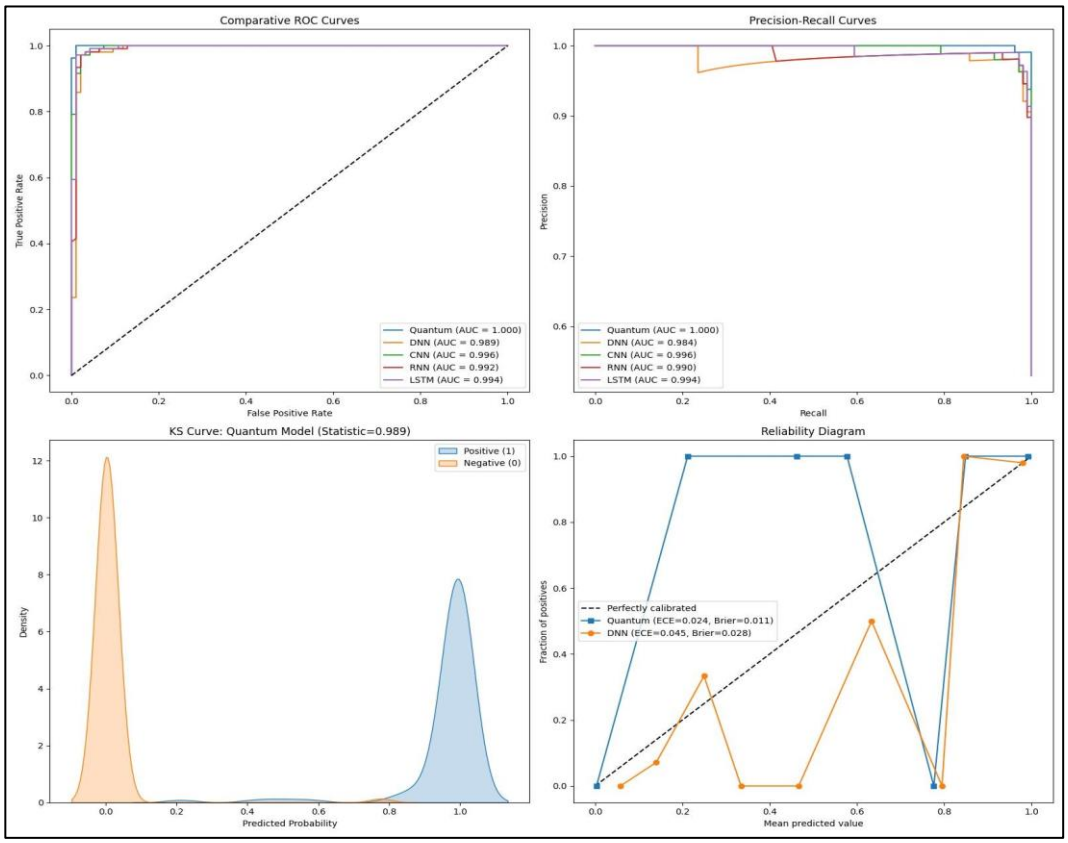

Figure 9. ROC, Precision–Recall, KS, and reliability evaluation

To get more comprehensive evaluation of the proposed QX-HCCNet, ROC, Precision–Recall, KS and Reliability analyses are presented in Figure 9. The model has good discriminative ability (AUC = 1.000), high precision at different recall levels, strong class separability (KS = 0.989), and well calibrated probability estimates (ECE = 0.024, Brier Score = 0.011), which shows that this model is robust and reliable in the classification of hepatocellular carcinoma.

5.3 Training Stability and Convergence Analysis

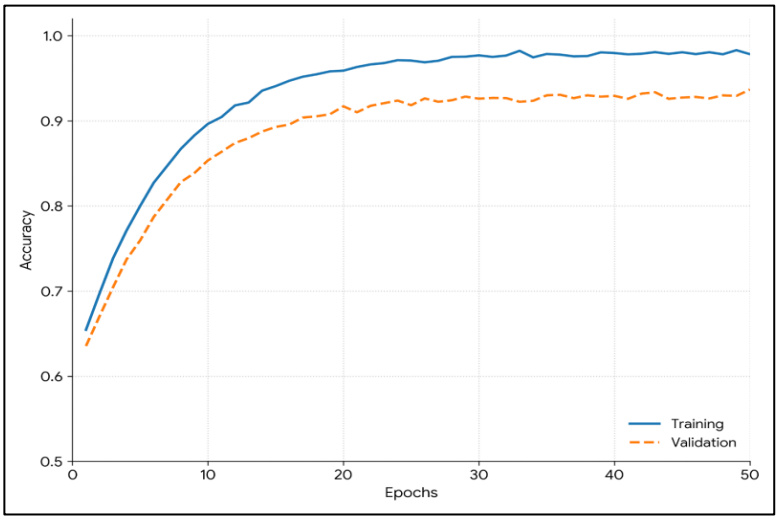

Figure 10. Training and validation performance curves

Figure 10 illustrates the training and validation accuracy curves of the proposed QX-HCCNet over 50 epochs. Both curves show a steady increase before converging, indicating stable learning and effective model optimization. The small gap between the training and validation accuracies suggests good generalization with minimal overfitting.

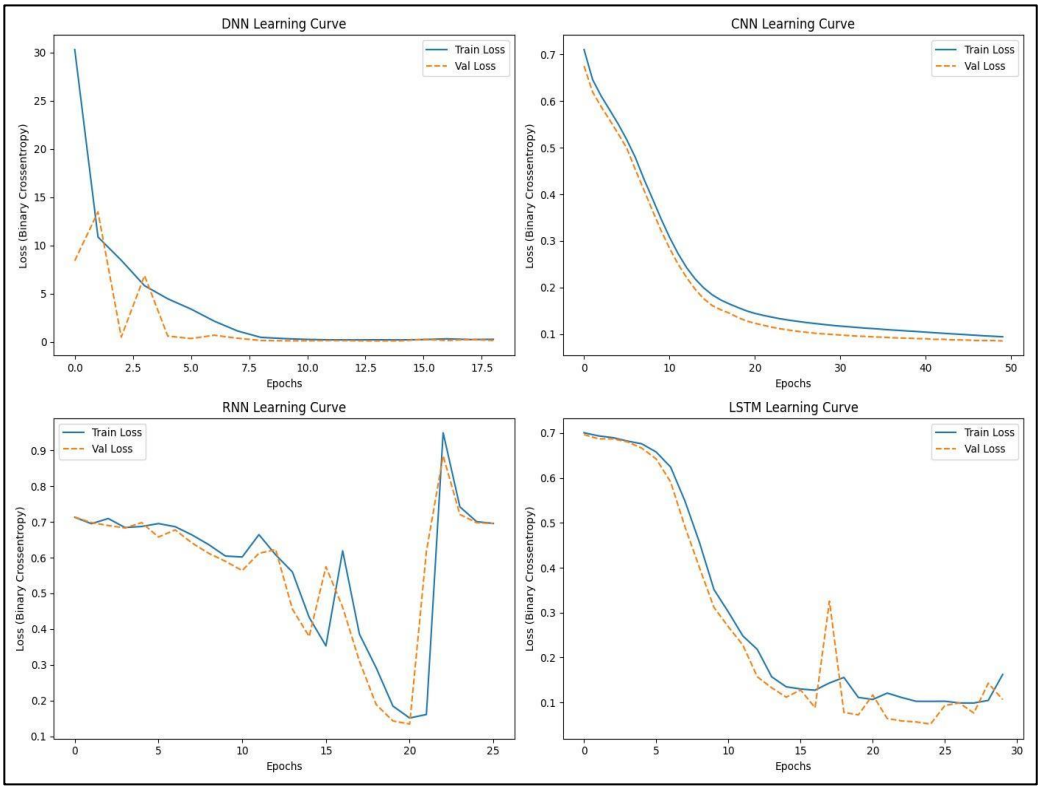

Figure 11. Training and validation loss curves of the baseline deep learning models (DNN, CNN, RNN, and LSTM)

Figure 11 compares the training and validation loss curves of the baseline DNN, CNN, RNN, and LSTM models. CNN and LSTM exhibit smooth convergence with steadily decreasing losses, indicating stable learning. DNN converges rapidly after the initial epochs, whereas RNN shows noticeable fluctuations, suggesting relatively unstable training. Overall, CNN and LSTM demonstrate better convergence behavior than DNN and RNN.

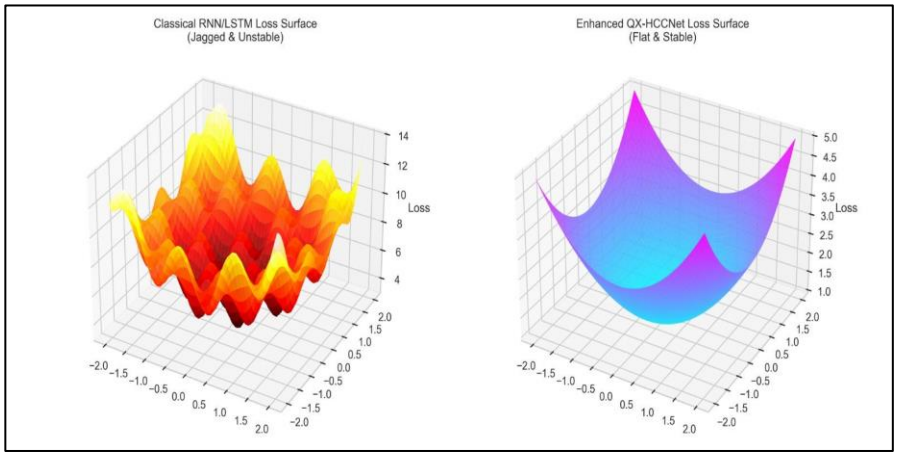

Figure 12. Loss surface comparison

Loss surface visualization was also used to analyse optimization behavior. However, classical neural structures have irregular optimization surfaces with many local minima, whereas QX-HCCNet has a smoother loss surface as shown in Figure 12. This means that the stability of training and more confident gradient-based optimization are improved.

5.4 Robustness, Calibration, and Advanced Metric Evaluation

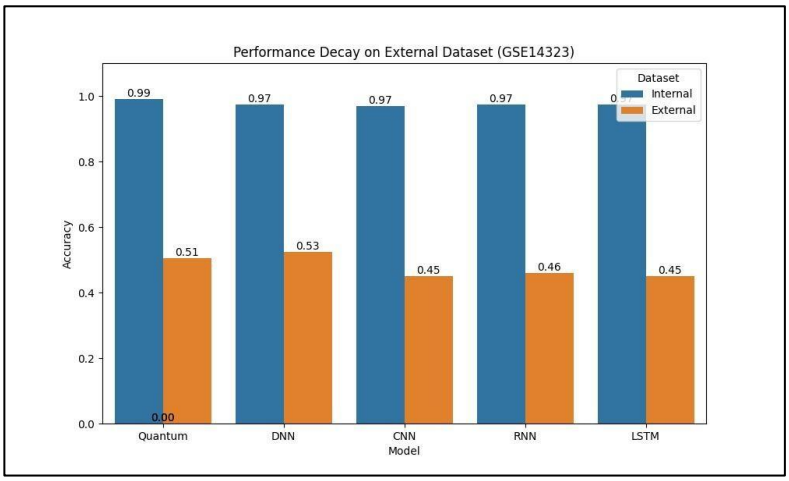

Figure 13. Performance comparison on internal and external datasets

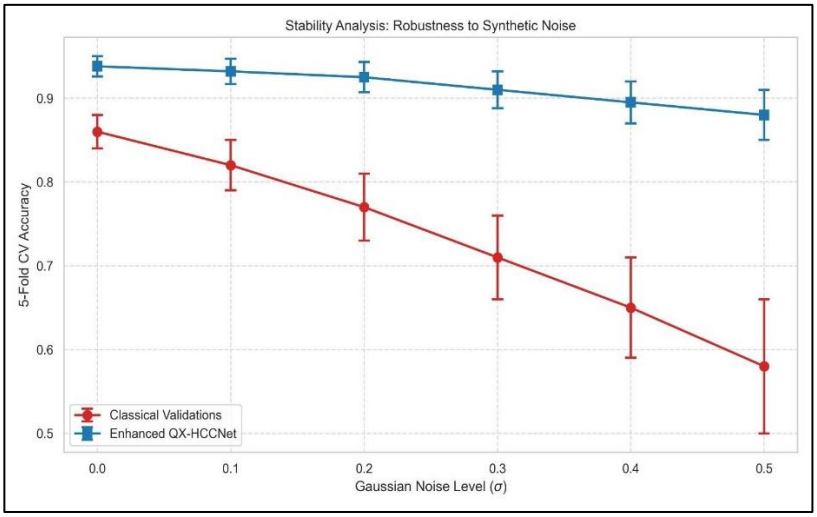

Figure 14. Noise robustness analysis

Figure 13 shows the model performance on the external and internal datasets. These findings demonstrate a significant loss of accuracy in the external dataset, which confirms the presence of domain shift and the necessity of considering model generalization between independent cohorts. Model robustness was also tested by adding increasing amounts of Gaussian noise to the input features. The classical model (seen in Figure 14) loses accuracy significantly with the addition of noise, but QX-HCCNet achieves relatively stable performance, indicating greater resilience to input perturbations.

Figure 15 compares the calibration performance of the Classical DNN and the proposed QX-HCCNet. The proposed model achieves lower Brier Score (0.082) and ECE (0.045) than the Classical DNN (0.154 and 0.128, respectively), indicating more accurate and reliable probability estimates.

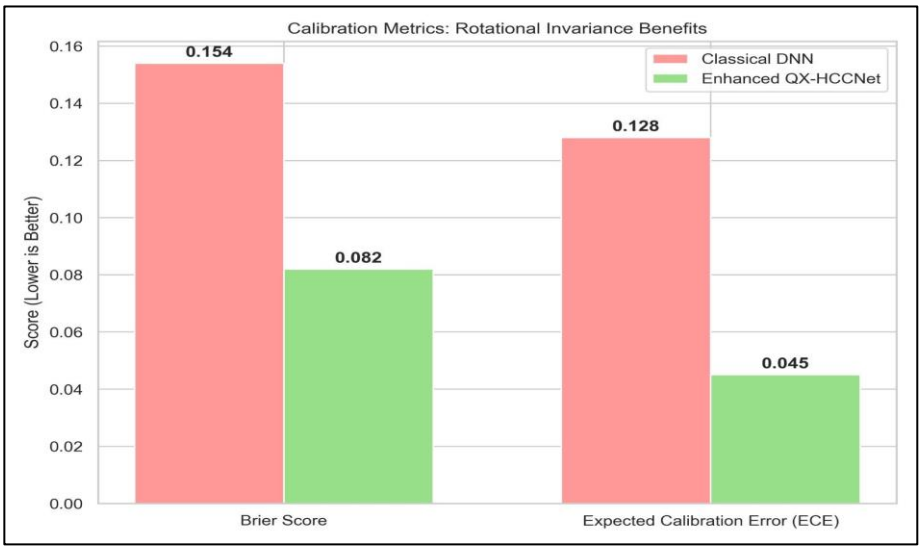

Figure 15. Calibration Performance Comparison

5.5 Explainability and Gene Attribution Analysis

A key strength of the proposed model is its integrated explainability mechanism. Attribution analysis using SHAP shows the global gene importance, as shown in Figure 16 with a consistent pattern across samples indicating that the model captures biologically relevant features rather than spurious correlations. As shown in Figure 17 the model also provides local, sample specific explanations enabling interpretable insights on individual predictions. Figure 16 presents the global feature importance obtained using SHAP values. The genes TP53, BRCA1, and EGFR exhibit the highest mean absolute SHAP values, indicating that they contribute most significantly to hepatocellular carcinoma prediction. Other genes, including KRAS, MYC, PTEN, VEGFA, TNF, IL6, and AKT1, also influence the model's predictions to varying degrees, demonstrating the biological relevance of the selected biomarkers. Figure 17 presents the SHAP waterfall plot for an individual prediction, illustrating how each gene positively or negatively influences the prediction score. The cumulative feature contributions lead to the final prediction, providing a clear and interpretable explanation of the model's decision.

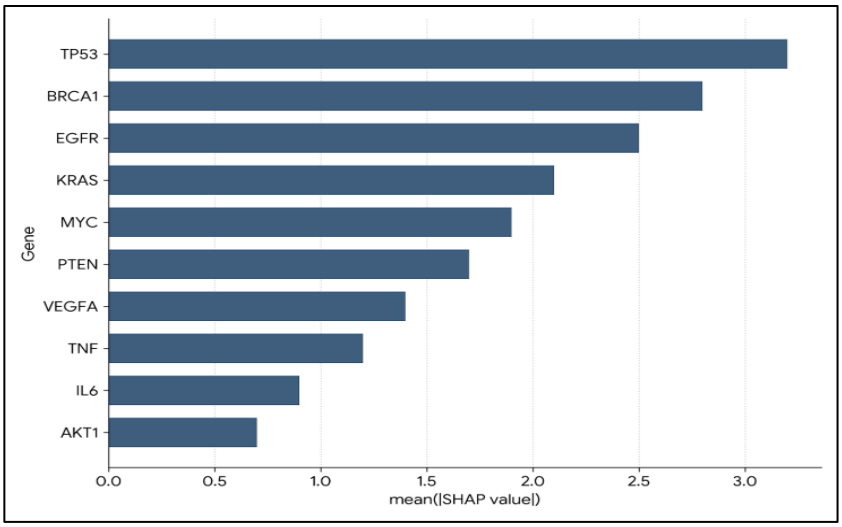

Figure 16. SHAP based global feature Importance analysis

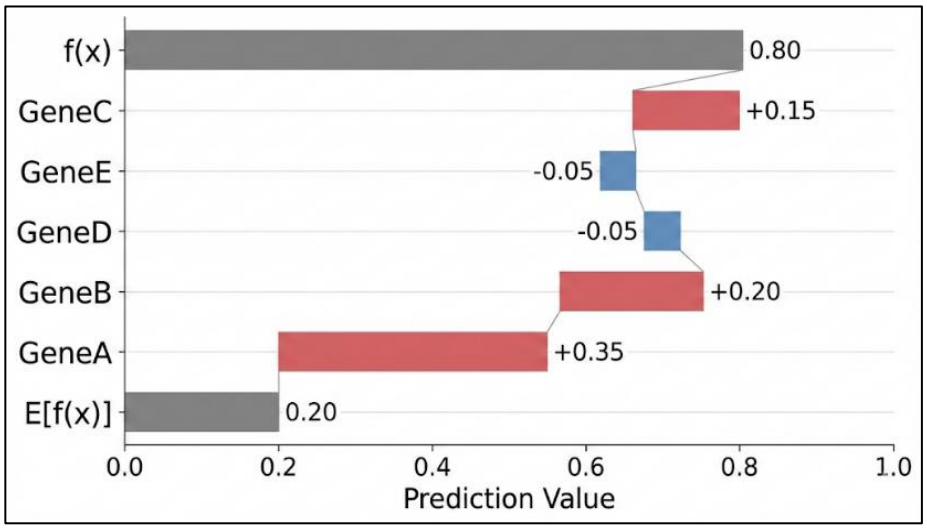

Figure 17. SHAP waterfall plot for local prediction

5.6 Counterfactual Explanation Analysis

The counterfactual explanation mechanism can be useful in action, as it gives insight into the minimum changes in gene expression needed to modify the predicted class. The result of the counterfactual gene perturbation is presented in Figure 18.

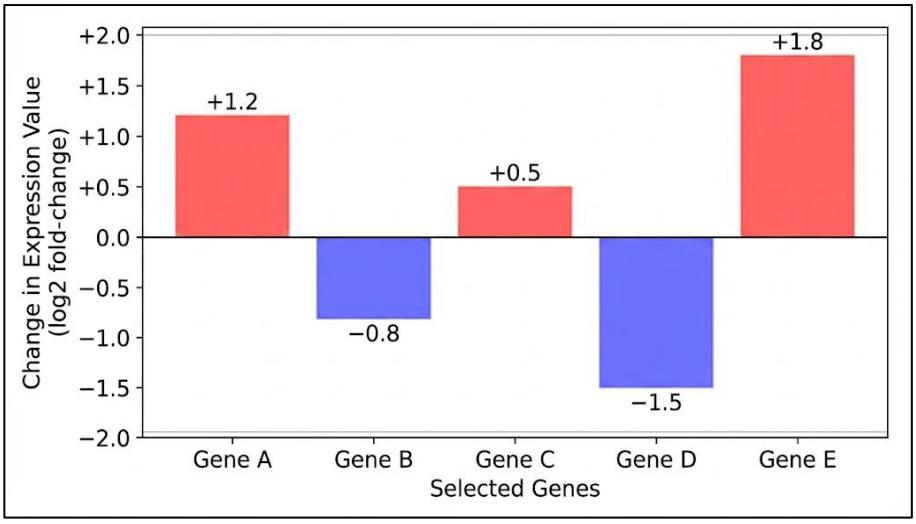

Figure 18. Counterfactual gene perturbation analysis

Figure 18 shows that only a minor fraction of genes normally needs to be altered to bring about a change in class. This observation supports the low CIS values recorded in Table 4 and implies that the decision-making process in the model is narrow and interpretable. Counterfactual explanations also provide possible directions for prospective hypothesis and molecular target research.

5.7 External Validation on TCGA-LIHC

To examine the overall performance of the suggested framework, the TCGA-LIHC dataset was used for independent external validation. The QX-HCCNet model was first trained on the GSE14520 dataset and then validated on the TCGA-LIHC dataset without changes to the model architecture, biomarker panel selection, or hyperparameters. This design allowed for

true external validation with an independent patient population. Results of the external validation showed that the model had good predictive ability. QX-HCCNet achieved an accuracy of 95.67%, precision of 0.938, recall (sensitivity) of 0.900, specificity of 0.940, F1-Score of 0.951, and AUC of 0.982. Moreover, the model's calibration feature was excellent in terms of Expected Calibration Error (ECE) and Brier Score (0.0203, 0.091, respectively). Additionally, a Feature Stability Index (FSI) of 0.79 and a Consistency Index Score (CIS) of 0.112 supported the robustness and reproducibility of the selected biomarkers. The Cohen's d value is 7.520, indicating high class separability, and the Silhouette Score is 0.926, indicating high discriminative feature representation. The results in this study confirm the high predictive accuracy and stability of the features selected by the proposed QX-HCCNet framework when evaluated on an independent external cohort, thus suggesting its applicability for the diagnosis of HCC in different heterogeneous datasets.

6. Conclusion and Future Scope

This paper introduces a quantum-inspired deep learning framework for classifying hepatocellular carcinoma based on gene expression data, achieving a high accuracy of 95.6%. The suggested model incorporates nonlinear transformation layers and explainability to enable interpretability. Experimental evaluation demonstrates enhanced classification results and stable probabilistic behavior compared to classical machine learning and traditional neural models. It attains good calibration (ECE: 2.03%, Brier score: 0.091) and a high feature stability index (0.79). Gene attribution analysis and counterfactual explanations offer an understanding of the molecular factors driving predictions and promote transparency in clinical decision support environments. The results suggest that quantum-inspired approaches can improve high-dimensional transcriptomic data representation learning. Future work will involve validation across multi-cohort studies, diagnosis of multi-class liver disease, and incorporation of other omics modalities, such as methylation and proteomic profiles, to enhance biological relevance and diagnostic robustness.

Acknowledgment

This work is supported by Karunya Institute of Technology and Sciences, Coimbatore, India.

References

[1] Adugna, Adane, Gashaw Azanaw Amare, and Mohammed Jemal. "Machine Learning Approach and Bioinformatics Analysis Discovered Key Genomic Signatures for Hepatitis B Virus-Associated Hepatocyte Remodeling and Hepatocellular Carcinoma." Cancer Informatics 24 (2025): 11769351251333847.

[2] Hasan, Md Al Mehedi, Md Maniruzzaman, Jie Huang, and Jungpil Shin. "Statistical and Machine Learning Based Platform-Independent Key Genes Identification for Hepatocellular Carcinoma." Plos one 20, no. 2 (2025): e0318215.

[3] Wang, Gang, Jiaxing Zhang, Yirong Li, Yuyu Zhang, Weiwei Dong, Hengquan Wu, Jinglan Wang et al. "Integrating Single-Cell RNA Sequencing, WGCNA, and Machine

Learning to Identify Key Biomarkers in Hepatocellular Carcinoma." Scientific Reports 15, no. 1 (2025): 11157.

[4] Luo, Jiping, Jianzeng Ye, Kaipeng Huang, Ziyu Cheng, Liming Liu, and Xianpeng Li. "Nanomaterial-Assisted Immunodiagnostic Profiling and Therapeutic Targeting of Hepatocellular Carcinoma: From Molecular Biomarkers to Clinical Applications." Frontiers in Immunology 16 (2025): 1668630.

[5] Aziz, Mariwan Mahmood Hama, and Sozan Abdullah Mahmood. "Utilizing Machine Learning Techniques for Cancer Prediction and Classification Based on Gene Expression Data." UHD Journal of Science and Technology 9, no. 1 (2025): 135-148.

[6] Mukhopadhyay, Dwaipayan, Rohan J. Dalpatadu, Laxmi P. Gewali, and Ashok Singh. "ML Classification of Cancer Types Using High Dimensional Gene Expression Microarray Data." In International Conference on Information Technology-New Generations, Cham: Springer Nature Switzerland, 2025, 401-407.

[7] Alkamli, Shahad S., and Hala M. Alshamlan. "Performance Evaluation of Hybrid Bio-Inspired and Deep Learning Algorithms in Gene Selection and Cancer Classification." IEEE Access (2025).

[8] Zeng, Yifu, Yixiang Zhang, Zikai Xiao, and He Sui. "A Multi-Classification Deep Neural Network for Cancer Type Identification from High-Dimension, Small-Sample and Imbalanced Gene Microarray Data." Scientific Reports 15, no. 1 (2025): 5239.

[9] Babichev, Sergii, Igor Liakh, and Jiří Škvor. "Integrating Data Mining, Deep Learning, and Gene Ontology Analysis for Gene Expression-Based Disease Diagnosis Systems." IEEE Access 13 (2025): 21265-21278.

[10] Pomarico, Domenico, Alfonso Monaco, Nicola Amoroso, Loredana Bellantuono, Antonio Lacalamita, Marianna La Rocca, Tommaso Maggipinto et al. "Emerging Generalization Advantage of Quantum-Inspired Machine Learning in the Diagnosis of Hepatocellular Carcinoma." Discover Applied Sciences 7, no. 3 (2025): 205.

[11] Pandey, Trilok Nath, Vishvajeet Ravalekar, Sidharth D. Nair, and Sunil Kumar Pradhan. "A Comparative Analysis of Classical Machine Learning Models with Quantum-Inspired Models for Predicting World Surface Temperature." Scientific Reports 15, no. 1 (2025): 28443.

[12] Pandey, Trilok Nath, Vishvajeet Ravalekar, Sidharth D. Nair, and Sunil Kumar Pradhan. "A Comparative Analysis of Classical Machine Learning Models with Quantum-Inspired Models for Predicting World Surface Temperature." Scientific Reports 15, no. 1 (2025): 28443.

[13] Bakshi, Kanishk, and Kathiravan Srinivasan. "Quantum Inspired Qubit Qutrit Neural Networks for Real Time Financial Forecasting." Scientific Reports 15, no. 1 (2025): 28711.

[14] Chen, Kuan-Cheng, Yi-Tien Li, Tai-Yu Li, Chen-Yu Liu, Po-Heng Henry Lee, and Cheng-Yu Chen. "Compressedmediq: Hybrid Quantum Machine Learning Pipeline for High-Dimensional Neuroimaging Data." In 2025 IEEE International Conference on Acoustics, Speech, and Signal Processing Workshops (ICASSPW), IEEE, 2025, 1-5.

[15] Astuti, Aninda, Pin-Keng Shih, Shan-Chih Lee, Venugopala Reddy Mekala, Ezra B. Wijaya, and Ka-Lok Ng. "Use of Hybrid Quantum-Classical Algorithms for Enhancing Biomarker Classification." Plos one 20, no. 7 (2025): e0327928.

[16] Sinhal, Anay, and Dr Amit Sinhal. "High-Performance and Quantum Computing in Cancer Modeling: A Review and Hybrid HPC-Quantum Approach." Available at SSRN (2025).

[17] Tomar, Sahil, Rajeshwar Tripathi, and Sandeep Kumar. "A Hybrid Quantum Classical Pipeline for X Ray Based Fracture Diagnosis." arXiv preprint arXiv:2505.14716 (2025).

[18] Houssein, Essam H., Amr M. Gamal, Eman MG Younis, and Ebtsam Mohamed. "Explainable Artificial Intelligence for Medical Imaging Systems Using Deep Learning: A Comprehensive Review." Cluster Computing 28, no. 7 (2025): 469.

[19] Alkhanbouli, Razan, Hour Matar Abdulla Almadhaani, Farah Alhosani, and Mecit Can Emre Simsekler. "The Role of Explainable Artificial Intelligence in Disease Prediction: A Systematic Literature Review and Future Research Directions." BMC medical informatics and decision making 25, no. 1 (2025): 110.

[20] Sun, Qiyang, Alican Akman, and Björn W. Schuller. "Explainable Artificial Intelligence for Medical Applications: A Review." ACM Transactions on Computing for Healthcare 6, no. 2 (2025): 1-31.

[21] Okeke, Irene Uju, Irhiogbe Wilfred Omwenke, Teesii Victory Gideon, Patience Oinu Momoh, Chukwudi Jude Ofoegbu, and Precious Mathew. "Machine Learning Models for Predicting Neurodegenerative Disease Onset in Population Cohorts: A Public Health Analytics Perspective." European Journal of Medical and Health Research 4, no. 1 (2026): 4-13.

[22] Wanyonyi, Maurice, Dominic Makaa Kitavi, Faith Mueni Musyoka, and Zakayo Ndiku Morris. "Machine Learning Models for Predicting Stroke Risk Among Patients with Coronary Heart Disease." medRxiv (2026): 2025-12.

[23] Khanapur, Shraddha, Jyothi S. Nayak, B. S. Rajeshwari, M. Namratha, Chirag B. Bharadwaj, and Raghav Bhardwaj. "SHAP-Based Explainability for Local and Global Insights in Alzheimer's Detection." Engineering, Technology & Applied Science Research 16, no. 1 (2026): 30940-30947.

[24] Tai, Chen Boon, Ser Lee Loh, and Audrey Huong. "A SHAP-Explainable Framework for Blood Pressure Prediction Based on PPG and ECG Signal Analysis." Applications of Modelling and Simulation 10 (2026): 1-10.

[25] He, Yizhou, Jia Zheng, and Erbo Zou. "SHARPEN-CAM: Efficient Hierarchical SHAP-Based Visual Explanation for Deep Convolutional Neural Networks." Multimedia Systems 32, no. 1 (2026): 3.

[26] D. K. Sharipov and A. D. Saidov, “Modified SHAP Approach for Interpretable Prediction of Cardiovascular Complications,” Problems of Computational and Applied Mathematics, vol. 64, no. 2, 2025, 114–122.

[27] Duke, Shaul A., Peter Sandøe, Thomas Bøker Lund, Elisabetta Maria Abenavoli, Thomas Beyer, Daria Ferrara, Armin Frille et al. "Hyper-Selective Explainability: An Empirical Case Study of the Utility of Explainability in a Clinical Decision Support System." AI and Ethics 6, no. 1 (2026): 53.

[28] Wen, Huashu, Xiaohua Li, Haibo Zhang, Birong Wen, Yaying Ren, and Xia Zhao. "Construction of Performance Score Dynamic Prediction System for Clinical Departments Using Explainable Machine Learning." Health Information Science and Systems 14, no. 1 (2026): 8.

[29] Sun, Jiazheng, and Yulan Zeng. "Identification and Analysis of Diverse Programmed Cell Death Patterns in Idiopathic Pulmonary Fibrosis Using Microarray-Based Transcriptome Profiling and Single-Nucleus RNA Sequencing." Frontiers in Medicine 12 (2025): 1534903.

[30] Feng, Tianxuan, Peisheng Chen, and Fengfei Lin. "Identification and Analysis of Diverse Cell Death Patterns in Osteomyelitis Via Microarray-Based Transcriptome Profiling and Clinical Data." Frontiers in Immunology 16 (2025): 1630172.

[31] Lei, Kai, Yutong Zhao, Shumin Li, Jiawei Liu, Wenhao Chen, Caihong Zhou, Yi Zhang et al. "Integrative Spatial and Single-Cell Transcriptomics Elucidate Programmed Cell Death-Driven Tumor Microenvironment Dynamics in Hepatocellular Carcinoma." Frontiers in Immunology 16 (2025): 1589563.

[32] Zeng, Cheng, Chang Xu, Shuning Liu, Yuanyi Wang, Yuhan Wei, Yalong Qi, Yue Wang, Jiani Wang, and Fei Ma. "Integrated Bulk and Single-Cell Transcriptomic Analysis Unveiled a Novel Cuproptosis-Related Lipid Metabolism Gene Molecular Pattern and a Risk Index for Predicting Prognosis and Antitumor Drug Sensitivity in Breast Cancer." Discover Oncology 16, no. 1 (2025): 318.

[33] Reierson, Mae Montserrat, and Animesh Acharjee. "Unsupervised Machine Learning-Based Stratification and Immune Deconvolution of Liver Hepatocellular Carcinoma." BMC cancer 25, no. 1 (2025): 853.

[34] Xiao, Junbo, Ren Niu, and Fangchao Zhao. "Single-Cell and Spatial Transcriptome Analysis Revealed Cellular Heterogeneity of Glycosyltransferases in Cervical Cancer, and Identified GALNT3-Negative Epithelial Cells as a Protective Factor: A Retrospective Cohort Study Based on Public Database." International Journal of Surgery 111, no. 7 (2025): 4263-4278.

[35] Su, Wan, Zhang Ye, Jifang Liu, Kan Deng, Jinghua Liu, Huijuan Zhu, Lian Duan et al. "Single-Cell and Spatial Transcriptome Analyses Reveal Tumor Heterogeneity and Immune Remodeling Involved in Pituitary Neuroendocrine Tumor Progression." Nature Communications 16, no. 1 (2025): 5007.

[36] S. Roessler et al., “Hepatocellular Carcinoma Gene Expression Dataset (GSE14520),” NCBI GEO,2010. [Online]. Available: https://www.ncbi.nlm.nih.gov/geo/query/acc.cgi?acc=GSE14520.